*International Journal of Minerals, Metallurgy and Materials*
*Volume 19, Number 9, Sep 2012, Page 812*
**DOI: 10.1007/s12613-012-0633-z**

# Microstructural and mechanical characteristics of Al-alloyed ductile iron upon casting and annealing

*N. Haghdadi*[1)], *B. Bazaz*[2)], *H.R. Erfanian-Naziftoosi*[1)], *and A.R. Kiani-Rashid*[1)]

1) Department of Materials Engineering, Faculty of Engineering, Ferdowsi University of Mashhad, 91775-111 Mashhad, Iran

2) School of Metallurgy and Materials Engineering, College of Engineering, University of Tehran, 11365-4563 Tehran, Iran

(Received: 23 July 2011; revised: 9 September 2011; accepted: 16 October 2011)

**Abstract:** Ductile iron containing 6.16wt% Al was produced to investigate the effects of aluminum on both its microstructure and hardness. Aluminum not only increases the nodule count and pearlite content but also improves the hardness in both sand mold and metal mold castings. Annealing treatments were conducted to attain a homogenous microstructure and improve high-temperature serviceability. A ferrite/carbide or ferritic matrix was gained depending on the annealing temperature. It is also discovered that annealing has inverse influences on the hardness of the bulk alloy and the ferrite phase. Although it causes a small decrease in the bulk hardness of the specimens, it leads to an increase in the microhardness of the ferrite. Micro-segregation of the alloying elements was also investigated by means of electron probe micro-analysis for the specimens with different annealing durations and the as-cast specimen as well. An optimum annealing time was proposed to result in the least amount of micro-segregation of aluminum and silicon between graphite nodules.

**Keywords:** cast iron; aluminum alloys; casting; annealing; microstructure; hardness

## 1. Introduction

Nodular iron is a member of the cast iron family which includes gray, malleable, white, and compacted graphite irons. The microstructure of ductile iron consists of spherical graphite nodules in a matrix of ferrite, pearlite, and cementite or a combination of these phases. These engineering materials have been used for a variety of applications due to their superior corrosion and wear resistance and excellent mechanical properties such as ductility and machineability, besides the high elastic modulus, high strength and good fatigue properties [1-5]. Thanks to the above advantages, they are successfully used to replace cast and forged steels in a variety of applications, thereby providing technical and economic advantages. Therefore, production of ductile iron has shown a sustained growth rate over the last four decades.

The microstructural properties of as-cast ductile iron are significantly influenced by the melting process, chemical composition, and cooling rate [1-5]. Aluminum and silicon have a similar effect on the iron-carbon alloy system; hence, attempts have been made to replace silicon by aluminum first of which was performed by Keep [6]. Keep showed that aluminum itself acts as an active precipitant of graphite in the absence of silicon. Recently, using aluminum in ductile iron has been widely demanded according to its desirable characteristics. Ductile iron has been the most economical candidate for elevated operating temperatures in the automotive industry. Moreover, in an industrial approach, there is an ongoing quest to reduce the overall weight of the components. Addition of aluminum makes possible the production of thin wall castings with lower weights [2-4, 6-10]. Kiani Rashid and Edmonds [7] have reported that for an as-cast ductile iron, the formation of an aluminum oxide layer acts as a diffusion barrier and reduces the rate of iron oxidation. As the amount of aluminum increases, the protective Al-rich layer can be formed in a shorter time and this, in turn, results in lower oxidation and decarburization rates. Reynauld and Roberge [10] have reported that ductile iron with a minimum silicon equivalent (SiE) content of 6wt% (SiE=Si+0.8Al) would not experience any oxidation. Furthermore, in less than 4wt% content, aluminum decreases

Corresponding author: N. Haghdadi E-mail: nima.hdd@gmail.com

the primary carbide stability while it increases the fineness of the pearlite and the strength of the iron consequently [2]. However, alloyed irons have not been exploited fully because of the difficulties encountered during casting.

Sand and metal are two types of mold media commonly used in the casting manufacturing process, and hence they have been the subject of numerous studies [11]. In the first part of this paper, microstructural characteristics and hardness of as-cast specimens are compared taking the mold media into account. Considering the fact that hardness usually causes poor machinability, greater amounts of pearlite and harder pearlite causes more difficulty in machining. Besides, segregation of the alloying elements causes inhomogeneity and has an adverse effect on the mechanical properties. In the case of ductile iron, it is believed that the segregation is relevant to the types of alloying elements present in the microstructure and also the nodule count [2]. Moreover, although the presence of the primary carbides and intermetallic compounds generates hard and strong regions, they can be detrimental to the ductility and other mechanical properties of the bulk material [12-13]. In addition, for pearlitic ductile iron, Reynauld and Roberge [10] have shown that, at the working temperature above 700°C, decomposition of pearlite to ferrite and $Fe_3C$ leads to surface spalling during processing. Therefore, it comes to mind that an appropriate annealing treatment would minimize the segregation of the alloying elements, dissolve and redistribute the intermetallics and also lead to the transformation of pearlite to ferrite and metastable $Fe_3C$. Moreover, it has been reported that by use of an appropriate annealing temperature, an adequate amount of activation energy can be provided, causing the metastable cementite to be transformed to ferrite and graphite [14] which causes a decrease in the density of ductile iron. According to the specific changes in the Fe-C binary phase diagram of ductile iron with the Al content more than 4.88wt%, which will be described later on, it is possible to perform an annealing treatment at the temperature as high as 980°C in order to eliminate or redistribute the primary carbides and intermetallic compounds, reduce the solute segregation of alloying elements and change the metastable microstructure components to thermally stable ones. In this regard, a part of the present study focuses on the microhardness and microstructural evolution upon annealing. To address the aforementioned speculation, samples were exposed to three different annealing temperatures for different periods of time. Electron probe micro-analysis (EPMA) was also employed to evaluate the micro-segregation of aluminum and silicon in the as-cast and annealed specimens.

Previous studies have revealed that austenitic regions decrease with the increase of Al content and in the case of cast iron containing more than 4.88wt% Al, the austenite zone (γ-loop) seems to be completely disappeared [2,15-17]. In this condition, at high temperature, there would be excess carbon in the matrix and dimensional stability during hot working will be achieved. Since the microstructural investigations have verified the vanishing of γ-loop in the present study, the high temperatures of 920, 950, and 980°C conventionally known as austenitizing temperatures are discussed as potential high annealing temperatures in this paper. Taking all the above into consideration, a new kind of this cast iron grade has been developed.

## 2. Experimental procedure

### 2.1. Melting

The melts were cast with a pouring temperature of approximately 1350°C by both green sand molds and metal molds. Standard 12.5 and 25 mm Y-block sand molds and metal molds were used. A bottom gating introduced the metal smoothly into the mold cavity to ensure a sound casting. The experimental ductile irons with the chemical composition given in Table 1 were produced in a Morgan gas-fired furnace (with a 25 kg capacity lift-out crucible) and a high-frequency melting plant of 20 kg capacity (with a tilting crucible). After melting, the iron was superheated to 1550°C and small pieces of solid aluminum were then plunged into the bottom of the liquid metal (Fig. 1).

**Table 1. Chemical composition of the experimental ductile cast iron, wt%.**

| C | Al | Si | Ni | Mn | P | S | Mg | Fe |
|---|---|---|---|---|---|---|---|---|
| 3.25 | 6.16 | 1.25 | 0.07 | 0.10 | 0.005 | < 0.005 | < 0.06 | Bal. |

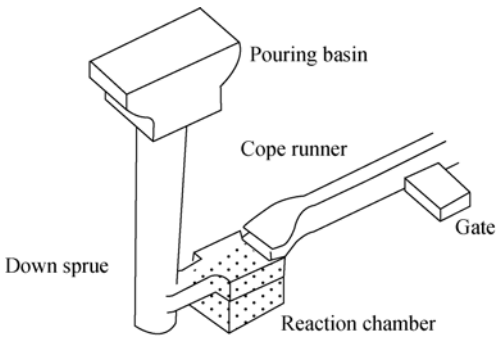


**Fig. 1. An in-mold spheroidizing gating arrangement for spheroidal irons.**

Adequate time was given to dissolve the aluminum completely in the molten metal. Following to aluminum, an Fe-SiMg (5wt% Mg) alloy was plunged into the liquid iron. The ejection of molten metal during the solution of magnesium was prevented by the use of special enclosed reaction vessels. Then, post-inoculation of ferrosilicon containing 75wt% Si was carried out in the crucible [18]. Finally, according to ASTM A897 M-90, the samples were prepared by sand mold and metal mold castings. After cutting and polishing the samples, quantitative measurements of the carbon content in the specimens were performed at Swinden Technology Centre of Corus Group PLC (formerly British Steel Ltd.). In order to analyze aluminum in the high Al content ductile iron, the atomic absorption spectrophotometry (AAS) method was applied at Hi Search Technology (HIST) of Birmingham University. To prevent any unwanted transformation, the samples were water cooled from the annealing temperature.

### 2.2. Sample preparation

For microstructural investigations, the samples were sectioned in proper size and polished by 80-1200 grinding paper. Initially, the samples were polished using diamond powders with a diameter of 1 μm and then the process continued using $Al_2O_3$ with the diameters of 0.3 and 0.05 μm. 2vol% nital solution was used as the etchant.

### 2.3. Microstructural examination

An optical microscope (OM, Olympus BX60MF5) equipped with a digital camera (JVC 10215670) was used to study the microstructure. A Cambridge Series 3 scanning electron microscope equipped with a Link 860 Series 1 EDX system and a Cambridge Series 4 scanning electron microscope were utilized for the characterization of microstructure. A working distance between 20 and 24 mm, an accelerating voltage of 20 kV, and the spot size between 4 and 6 nm were applied. In addition, image analysis was performed by the MIP image analyzing software (MIP is a registered trade mark for the metallographic image processing software developed in Nahamin Pardazan Asia Co. at the Ferdowsi University of Mashhad). XRD analysis was conducted using Cu $K_\alpha$ target radiation. An automated Philips ADP1700 diffractometer, operated at 40 kV and 20 mA over $2\theta$ values ranging from 15 to 135°, was used to detect the reflection of interest. Moreover, microanalysis investigations were performed using an electron probe micro analyzer (EPMA, CAMECA SX-50) equipped with a wave length dispersive X-ray spectrometer (WDS) and an energy dispersive spectrometer (EDS), to determine the distribution of Si and Al in the samples during solidification and annealing.

### 2.4. Hardness measurement

Microhardness measurements were carried out using a Vickers Engineering Group Vickers hardness machine at a load of 245 mN on the polished samples, and the hardness of the specimens was measured by a Universal Koopa machine at a load of 1.47 kN. A mean of five measurements was made for each sample.

## 3. Results and discussion

### 3.1. As-cast condition

Microstructures of the specimens observed by OM before etching are shown in Fig. 2. Figs. 2(a) and 2(b) illustrate the microstructures of sand mold and metal mold cast specimens, respectively. From these micrographs, it can be seen that a large amount of graphite in both specimens is spherical, and this is more evident in the metal mold sample.

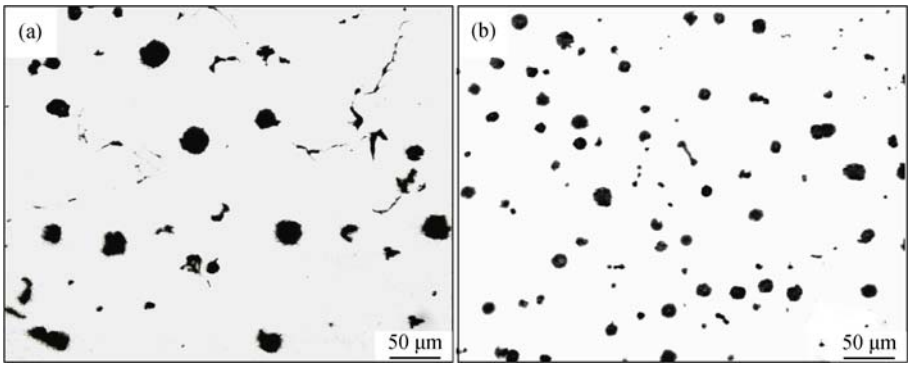


**Fig. 2. OM micrographs of the examined specimens prior to etching: (a) sand mold; (b) metal mold.**

Lower cooling rate in sand mold could lead to the rejection of carbon from graphite nodules. In addition, bigger size and particular arrangement of graphite in sand cast specimens may cause graphite nodules to meet one another

resulting in non-spherical graphite. This is why higher volume fractions of nodular graphite are observed in metal mold specimens. Microstructural examinations revealed that graphite has a more uniform distribution in metal mold specimens which brings about homogeneity and superior mechanical properties. Comparative results of the nodular graphite percent, degree of nodularity, and average nodule diameter of graphite for the two specimens are reported in Table 2. The high percentage of nodular graphite in comparison with conventional ductile iron is related to the presence of Al. Aluminum carbides, nitrides, and oxides are appropriate sites for graphite nucleation [2-3]. Smaller nodule size of graphite in metal mold specimens is due to the higher amount of graphite nuclei, and this in turn is attributable to higher undercooling. The radius of graphite nodules is a function of time ($R \propto (Dt)^{0.5}$, where $R$ is the radius of graphite nodule, $D$ the diffusion coefficient of carbon, and $t$ the solidification time). Therefore, higher rates of solidification in metal molds result in smaller nodule size. Fig. 3 shows the OM micrographs of the specimens after etching. The microstructures seem to be identical, and it is almost obvious that microstructures of the as-cast samples are free of $Fe_3C$ carbides. Although due to its FCC crystal structure, aluminum is expected to be an austenite stabilizer, it appears to accelerate the formation of pearlite. Generally speaking, elements which increase the interval between eutectic stability and instability temperature promote graphite formation; while elements which decrease this interval promote carbide formation. Therefore, since Al increases the mentioned interval, the formation of carbides becomes difficult [19]. In addition, aluminum acts as an inoculant for graphite, and consequently, the probability of carbide formation is noticeably decreased. In previous studies, it has been revealed that aluminum contents below 4wt% and above 10wt% cause graphite and carbides to be stabilized in the cast iron, respectively [20]. Comparing the results of this study with studies on irons with different contents of Al [19], cast iron containing 6.16wt% Al shows a graphite stabilizing behavior similar to that of the former category. The contents of various constituents in the microstructure for the investigated irons are reported in Table 3.

**Table 2. Characteristics of graphite in metal mold and sand mold specimens**

| Mold | Graphite nodules characteristics | | |
|---|---|---|---|
| | Nodular graphite / vol% | Nodularity / % | Average graphite diameter / μm |
| Sand | 69 | 81 | 14.4 |
| Metal | 87 | 89 | 11.6 |

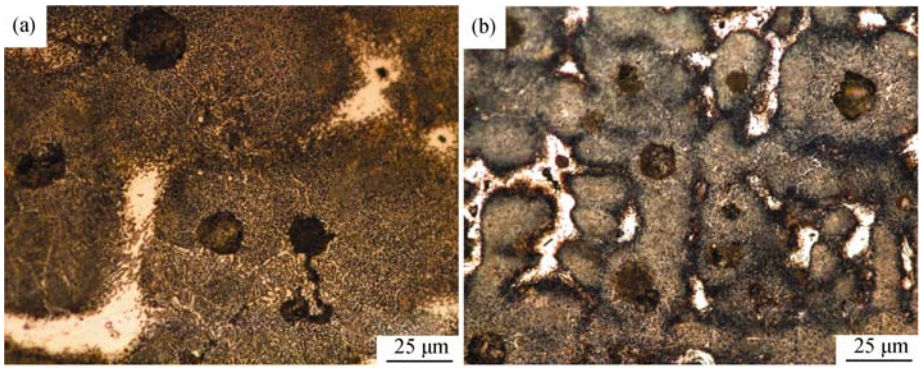


**Fig. 3. OM micrographs of the examined specimens etched in 2vol% nital: (a) sand mold; (b) metal mold.**

**Table 3. Microstructural characteristics of the specimens solidified in the metal mold and sand mold**

| Mold | Microstructural characteristics | | |
|---|---|---|---|
| | Ferrite / vol% | Pearlite / vol% | Graphite / vol% |
| Sand | 8.9 | 85.3 | 5.8 |
| Metal | 7 | 87.4 | 5.6 |

It is obvious that in both molds, the volume fraction of pearlite is significantly more than that of pearlite in non-Al containing ductile iron [19]. This can be attributed to two effects: one is the effect of Al as a pearlite stabilizer during the eutectic transformation which leads to an increase in the volume fraction of pearlite and a decrease in that of ferrite; the other is the dependency of ferrite formation on long range diffusion of carbon when pearlite formation needs just short range diffusion of carbon. In fact, high Al-containing regions around graphite act as a diffusion barrier and prevent the diffusion of carbon into the graphite [2, 21]. There are more graphite nodules in metal molds in comparison with sand molds limiting the carbon diffusion to graphite. Hence, the formation of pearlite as a phase which contains

more carbide is facilitated in metal molds. Moreover, since pearlite needs not as long times as ferrite to be nucleated and grown, more amount of pearlite seen in metal mold casts can be justified.

Compared to sand molds, metal molds facilitate the heat flow, leading to a finer grain structure. Since austenite grain boundaries are the preferential sites for pearlite nucleation, casting in metal molds provides more suitable sites for pearlite nucleation which results in more pearlite content with finer grain morphology. Microhardness of different phases in the specimens is reported in Table 4. It is discovered that the hardness is peculiarly more than usual. The positive effect of more nodule counts on hardness is in contrast with the findings of Hsu and his co-workers [22].

**Table 4. Microhardness of phases in cast iron specimens solidified in metal mold and sand mold**

| Mold | Microhardness, Hv | |
|---|---|---|
| | Pearlite | Ferrite |
| Sand | 359 | 238 |
| Metal | 365 | 276 |

It sounds as if the increased ferrite and pearlite hardness is due to the fineness of pearlite layers and the production of Al-Fe-C solid solutions, primary carbides, and intermetallic compounds. Harder phases in metal mold specimens can be justified with their finer microstructure. Higher undercooling and nodule count contribute to the achievement of a finer microstructure [23]. Besides, higher amounts of solute elements in the solid solution state and also higher amounts of intermetallics lead to an increase in the hardness of different phases in metal mold castings. XRD analysis was conducted to investigate these phases. Fig. 4 shows an XRD pattern of the sample. In addition to the main phases such as α-ferrite and $Fe_3C$, other Al-containing compounds were observed. One peak of each compound has been marked in the Fig. 4, and complementary results are given in the table shown therein. Moreover, based on the XRD results, an increase in the lattice parameter of ferrite (Table 5) and $Fe_3C$ (Table 6) is observed by increasing the Al content which is due to the presence of alloying elements specially aluminum as a solute.

### 3.2. Effect of annealing

Microstructures of the specimens after 1 h annealing at different temperatures are shown in Fig. 5. As seen in Figs. 5(a), 5(b), and 5(d), primary carbides and intermetallics are observed to disperse in the ferrite/carbide matrix, while

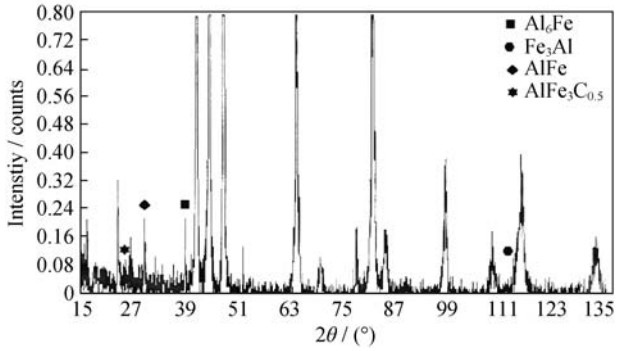


| Phase | 2θ / (°) |
|---|---|
| $AlFe_3C_{0.5}$ | 41.66, 48.26, 70.60, 23,58 |
| AlFe | 44.37, 81.50, 30.91, 64.17 |
| $Fe_3Al$ | 44.18, 80.92, 113.82, 63.99 |
| $Al_6Fe$ | 42.36, 48.61, 38.87, 45.26 |

**Fig. 4. XRD pattern of the examined specimen.**

**Table 5. Lattice parameter of ferrite in the examined specimen compared to ductile irons with different contents of aluminum nm**

| Alloy | Lattice parameter | |
|---|---|---|
| | Sand mold | Metal mold |
| 0.48wt% Al-3.68wt% C [2] | 2.8661 | 2.8679 |
| 2.11wt% Al-3.55wt% C [2] | 2.8668 | 2.8698 |
| 6.16 wt % Al-3.25wt% C | 2.8706 | 2.8735 |

**Table 6. Lattice parameter of $Fe_3C$ in the examined specimen compared to ductile irons with different contents of aluminum/nm**

| Alloy | Lattice parameter | |
|---|---|---|
| | Sand mold | Metal mold |
| 0.48wt% Al-3.68wt% C [2] | 1.04 | 1.41 |
| 2.11wt% Al-3.55wt% C [2] | 1.19 | 1.73 |
| 6.16wt% Al-3.25wt% C | 1.44 | 1.78 |

pearlite is absent. It could be rationally considered that the pearlite has decomposed to ferrite and $Fe_3C$ while not a considerable change in volume fraction of graphite has occurred. It is concluded that 920 and 950°C provide the activation energy only for the pearlite to ferrite and $Fe_3C$ decomposition, but not for $Fe_3C$ to graphite and ferrite. Fig. 5(c) is the microstructure of iron after holding at 980°C for 1 h. The metastable carbide has transformed to ferrite and graphite; hence there is a higher volume fraction of both ferrite and graphite compared to the as-cast conditions. According to the water cooling of specimens, the absence of martensite and/or bainite in the microstructures is attributed to the absence of the γ region in the phase diagram of the examined

specimens. Accordingly, the simulation results applying the MTDATA software show the vanishing of the γ loop from the phase diagram of ductile iron in the presence of 6.16wt% Al (Fig. 6) [16]. It is difficult to quantify the volume fraction and distribution of the mentioned hard phases and compounds in the matrix in Fig. 5, but it is likely that the increase of annealing temperature leads to the decrease in their volume fraction and accumulation. It is to be noticed that these phases are formed during casting, and it is not easy and sometimes impossible to eradicate them with annealing; however, their partial dissolution and redistribution may lead to more homogeneity.

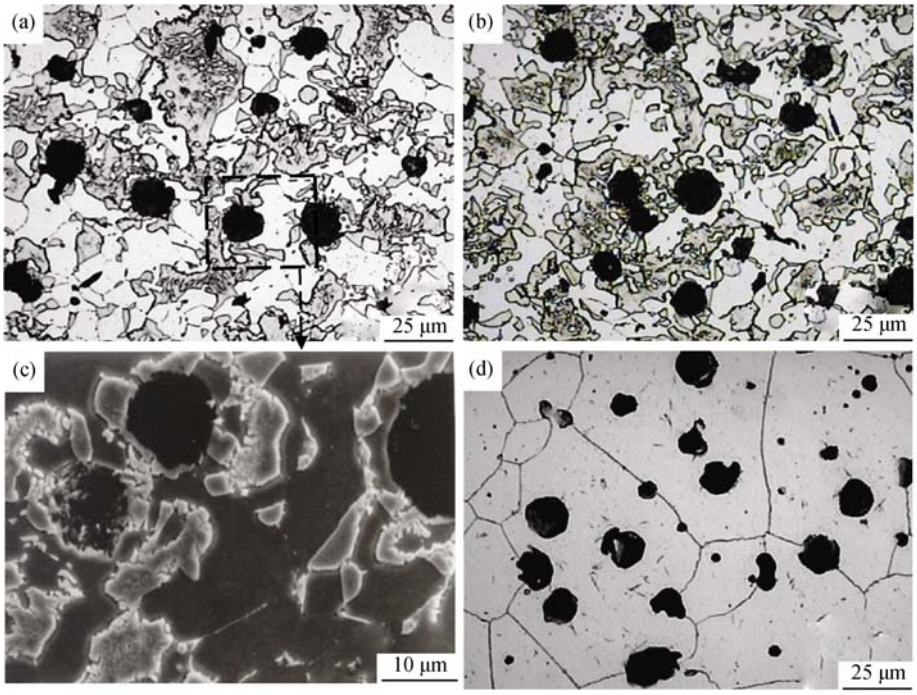


**Fig. 5. Microstructures of the examined iron after annealing for 60 min at 920°C (a) and (c), 950°C (b), and 980°C (d).**

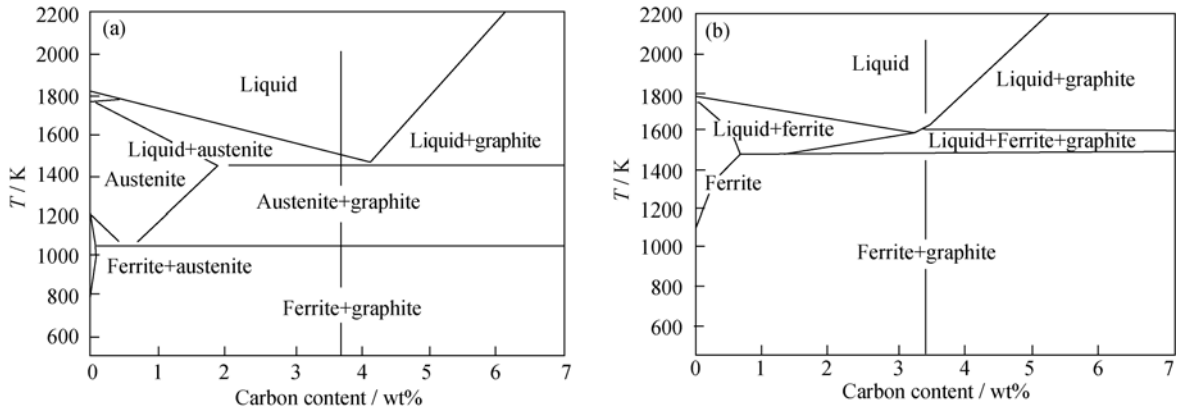


**Fig. 6. Typical binary Fe-C phase diagram (a) and predicted binary Fe-C phase diagram (b) with 6.16wt% Al [16].**

Electron probe micro-analysis (EPMA) images show the segregation patterns of Al and Si. High amounts of Al are seen near the graphite nodules, while Si tends to accumulate in the inter-granular regions rather than the nodule/matrix interface (Fig. 7).

Fig. 8 shows the EPMA images of Al and Si distribution in the microstructures of specimens together with the contents of Al and Si measured along single lines between the adjacent graphite nodules after annealing at 920ºC for different holding times. Comparing Figs. 7 and 8, it is observed that different regions of the cast alloy exhibit similar trends in the segregation of Si and Al. It is believed that micro-segregation occurs due to the reasons such as differences in density and solidification properties of different

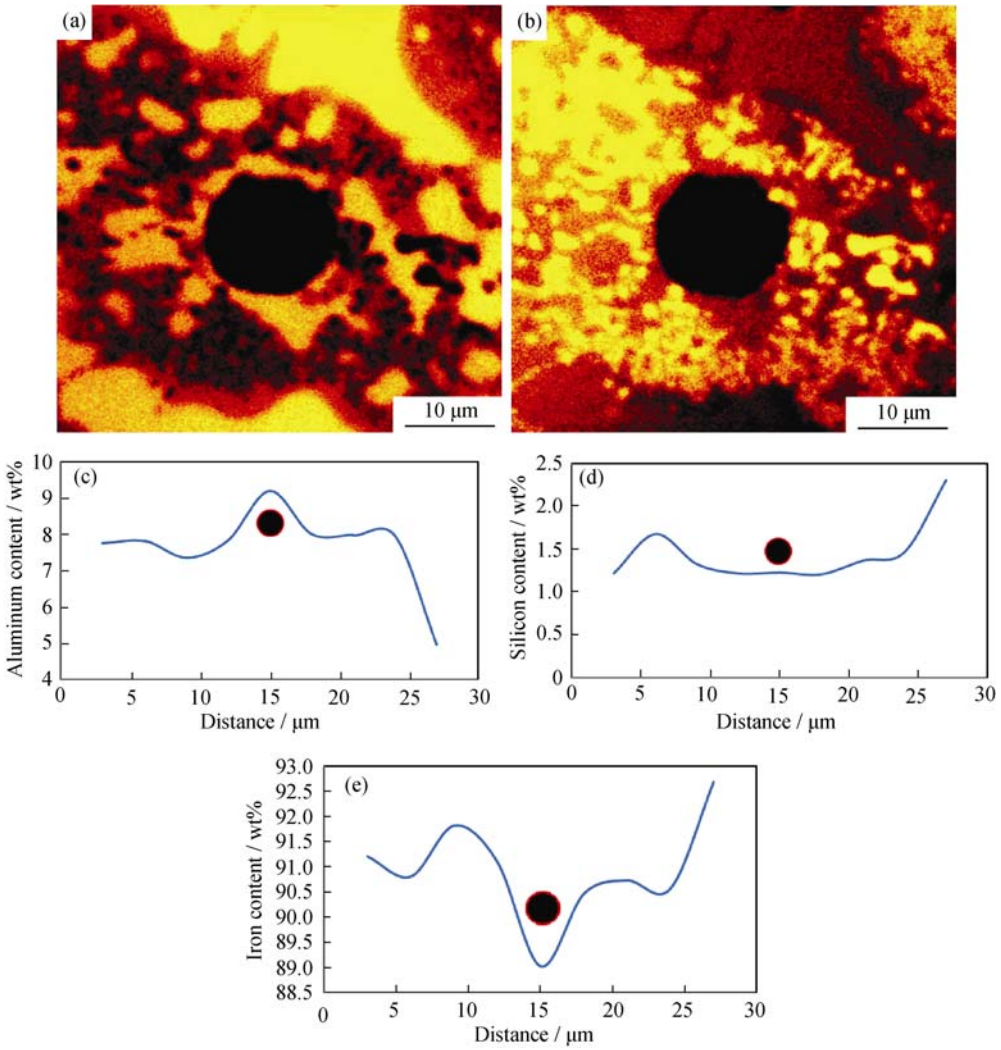


**Fig. 7. EPMA maps of (a) aluminum and (b) silicon in the metal mold cast specimen. Line concentration profile of (c) Al, (d) Si and (e) Fe.**

elements in the alloy. The presence of Al as a low density element can remarkably influence the micro-segregation during solidification. The results indicate that annealing effectively increases the homogeneity of the microstructures and a high degree of homogeneity is achieved for the 120-min annealed specimen. Generally, the migration of alloying elements is due to chemical potential gradient, which continues to reach an equilibrium thermodynamic condition and eliminates the difference in chemical potential.

Similar trends during holding at this temperature have been observed in irons with different levels of Al [2]. It has been seen that by increasing the holding time, the homogeneity of iron between graphite nodules increases and leads to a lower gradient of Al and Si. Contrary to our results, Bayati and Elliott [24] reported that for ductile iron containing 3.52wt% C, 2.64wt% Si, 0.67wt% Mn, 0.25wt% Mo, and 0.25wt% Cu held for 120 min at 920°C (austenitizing temperature for their iron), the matrix was heterogeneous and the segregation of alloying elements established during solidification was not removed completely. These opposite results can be related to the different annealing behaviors of Al in the experimental iron compared to Mn, Mo, and Cu in their alloy.

Accordingly, lower hardness is expected for the samples annealed at higher temperature. This became more evident when the hardness measurements were carried out. The obtained hardness results are reported in Table 7. At higher annealing temperature, it sounds that the partial dissolution of hard compounds and phases during annealing and their redistribution in the ferrite matrix during cooling causes an increase in the microhardness of ferrite. Increased microhardness for ferrite can also be related to the formation of Fe-Al intermetallics within ferrite grains.

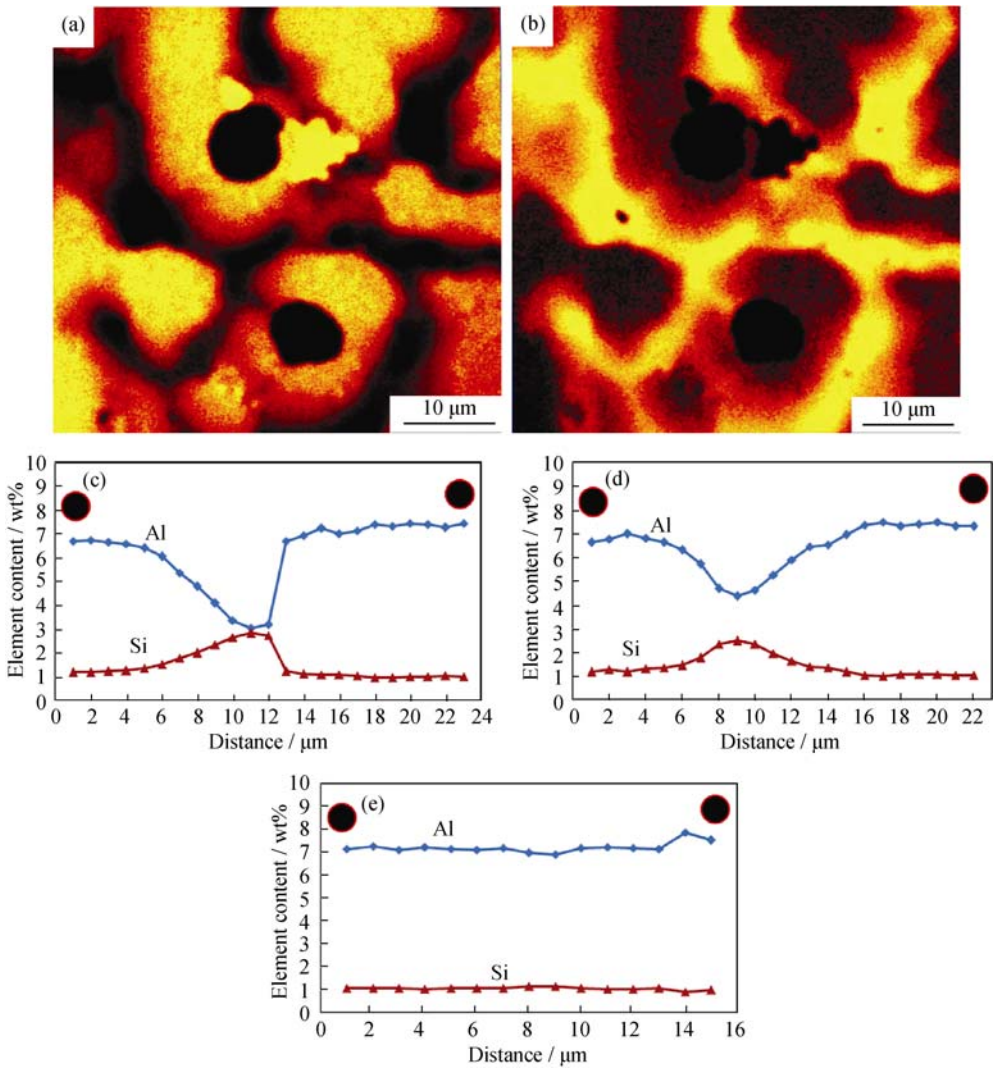


**Fig. 8. EPMA maps of aluminum (a) and silicon (b) of the examined iron in as-cast conditions. Al and Si contents between two nodules after annealing at 920°C for 10 min (c), 60 min (d), and 120 min (e).**

**Table 7. Hardness of the specimens and microhardness of ferrite in each specimen after annealing for 60 min**

| Annealing temperature / ºC | Hardness of the bulk sample, Hv | Microhardness of ferrite, Hv |
|---|---|---|
| 920 | 473 | 278 |
| 950 | 458 | 286 |
| 980 | 308 | 325 |

Previous studies have demonstrated that higher austenitizing temperature leads to cast iron with higher hardness [25]. Being in contrast with the previous reported results, the hardness values also indicate that γ-loop has vanished in ductile iron containing 6.16wt% Al in this study, leading to improved high temperature serviceability of the examined iron.

## 4. Conclusions

(1) Compared to conventional Fe-Si-C ductile irons, the 6.16wt% Al containing ductile iron showed an increasing trend in both the nodule count and the pearlite content. Metal mold specimens exhibited finer nodules with a more uniform distribution and higher hardness rather than sand mold specimens. Peculiar high hardness values for ferrite were achieved due to the presence of aluminum and silicon as solutes in ferrite, which is proved by the expansion of the ferrite lattice in the specimen with higher amounts of Al. Regarding the annealing treatment, the pearlite→ferrite+$Fe_3C$ transformation at 920 and 950ºC and $Fe_3C$→ferrite+graphite at 980ºC were observed. It was seen that higher annealing temperatures cause a decrease in the hardness of bulk specimens. On the other hand, annealing caused an in-

crease in the microhardness of ferrite.

(2) Electron probe micro-analysis showed that annealing is an effective treatment to decrease the concentration gradient of Al and Si between adjacent graphite nodules. According to the results, during annealing at 920°C, 120 min is long enough for the homogeneity to be reached.

(3) According to the results of the present study, it seems that the presence of 6.16wt% aluminum in the composition would lead to γ-loop vanishing in the phase diagram of this ductile iron which is in agreement with the earlier predictions of the authors.

## Acknowledgments

The authors would like to thank Prof. D.V. Edmonds (Materials Department of the University of Leeds) for his valuable support in EPMA.

## References

[1] J.R. Davis, *ASM Specialty Handbook: Cast Irons*, ASM International, 1996.

[2] A.R. Kiani-Rashid, *The Influence of Aluminum and Heat Treatment Conditions on Austempered Ductile Irons* [Dissertation], University of Leeds, Leeds, 2000.

[3] S.M.A. Boutorabi, The Austempering Kinetics, Microstructure and Mechanical Properties of Spheroidal Graphite Unalloyed Aluminum Cast Iron [Dissertation], University of Birmingham, Birmingham, 1991.

[4] A.R. Kiani-Rashid and D.V. Edmonds, Microstructural characteristics of Al-alloyed austempered ductile irons, *J. Alloys Compd.*, 477(2009), p.391.

[5] H.R. Abedi, A. Fareghi, H. Saghafian, and S.H. Kheirandish, Sliding wear behavior of a ferritic-pearlitic ductile cast iron with different nodule count, *Wear*, 268(2010), p.622.

[6] W.J. Keep, The influence of aluminum upon cast iron, [in] *Annual Meeting of the American Association for the Advancement of Science*, Detroit, 1888.

[7] A.R. Kiani Rashid and D.V. Edmonds, Oxidation behaviour of Al-alloyed ductile cast irons at elevated temperature, *Surf. Interface Anal.*, 36(2004), p.1011.

[8] M.M. Haque, Investigation on properties and microstructures of spheroidal graphite Fe-C-2Si and Fe-C-2Al cast irons, *J. Mater. Process. Technol.*, 191(2007), p.360.

[9] K.M. Pedersen and N.S. Tiedje, Graphite nodule count and size distribution in thin walled ductile cast iron, *Mater. Charact.*, 59(2008), p.1111.

[10] A. Reynauld and J.L. Roberge, Application of high temperature spheroidal graphite cast irons in exhaust manifolds, *Fonderie Fondeur d'Aujourd'hui*, 182(1999), p.37.

[11] D.M. Stefanescu, *ASM Metals Handbook Volume 15: Casting*, ASM International, 1988.

[12] M. Nili-Ahmadabadi and M. Mosallaiee-Pour, Homogenization of ductile iron using partial melting aided by modeling, *Mater. Sci. Eng. A*, 373(2004), p.309.

[13] J. Lacaze, Solidification of spheroidal graphite cast irons: III. Microsegregation related Effects, *Acta Mater.*, 47(1999), p.3779.

[14] B. Black, G. Burger, R. Logan, R. Perrin, and R. Gundlach, Microstructure and dimensional stability in Si-Mo ductile irons for elevated temperature applications, [in] *International Body Engineering Conference Exhibition and Automotive Transportation Technology Congress*, SAE International, No.10, 2002, p.363.

[15] A.R. Kiani-Rashid, Influence of austenitising conditions and aluminum content on microstructure and properties of ductile irons, *J. Alloys Compd*., 470(2009), p.323.

[16] A.R. Kiani-Rashid, The influence of Al content on the Fe-C-Al-Si equilibrium phase diagrams, *J. Metall. Mater. Eng.*, 21(2009), p.89.

[17] A.R. Kiani-Rashid and D.V. Edmonds, Phase transformation study of aluminum-containing ductile cast irons by dilatometry, *Mater. Sci. Eng. A*, 481-482(2008), p.752.

[18] J.R. Brown, *Foseco Ferrous Foundryman's Handbook*, Butterworth-Heinemann, 2000, p.70.

[19] A. Shayesteh-Zeraati, H. Naser-Zoshki, and A.R. Kiani-Rashid, Microstructural and mechanical properties (hardness) investigations of Al-alloyed ductile cast iron, *J. Alloys Compd.*, 500(2010), p.129.

[20] E.U. Petitbon and J.F. Wallace, Aluminum alloyed gray iron: Properties at room and elevated temperatures, *AFS Cast Met. Res. J.*, 9(1973), p.127.

[21] A.R. Kiani-Rashid and M.A. Golozar, Microscopic segregation pattern of Al and Si in matrix microstructure of cast irons with spherical graphite, *Esteghlal J.*, 2(2003), p.177.

[22] C.H. Hsu, M.L. Chen, and C.J. Hu , Microstructure and mechanical properties of 4% cobalt and nickel alloyed ductile irons, *Mater. Sci. Eng. A*, 444(2007), p.339.

[23] L.C. Kumruoglu, Mechanical and microstructure properties of chilled cast iron camshaft: Experimental and computer aided evaluation, *Mater. Des.*, 30(2009), p.927.

[24] H. Bayati and R. Elliott, Relationship between structure and mechanical properties in high manganese alloyed ductile iron, *Mater. Sci. Technol*., 11(1995), p.284.

[25] J. Krawvzjyk, P. Bala, and J. Pacyna, The effect of carbide precipitate morphology on fracture toughness in low-tempered steels containing Ni, *J. Microsc*., 237(2010), p.411.